

Article

Comparison of Physicochemical Properties of Fly Ash Precursor, Na-P1(C) Zeolite–Carbon Composite and Na-P1 Zeolite—Adsorption Affinity to Divalent Pb and Zn Cations

Rafał Panek ^{1,*}, Magdalena Medykowska ^{2,*}, Katarzyna Szewczuk-Karpisz ³ and Małgorzata Wiśniewska ²

¹ Department of Geotechnical Engineering, Faculty of Civil Engineering and Architecture, Lublin University of Technology, Nadbystrzycka 40, 20-618 Lublin, Poland

² Department of Radiochemistry and Environmental Chemistry, Faculty of Chemistry, Maria Curie-Skłodowska University in Lublin, M. Curie-Skłodowska Sq. 3, 20-031 Lublin, Poland; wisniewska@hektor.umcs.lublin.pl

³ Institute of Agrophysics, Polish Academy of Sciences, Doświadczalna 4, 20-290 Lublin, Poland; k.szewczuk-karpisz@ipan.lublin.pl

* Correspondence: r.panek@pollub.pl (R.P.); m.medykowska@poczta.umcs.lublin.pl (M.M.)

Abstract: Considering the growing needs of environmental remediation, new effective solutions should be sought. Therefore, the adsorbed amounts of heavy metal ions, such as lead(II) and zinc(II), on the surface of high-carbon fly ash (HiC FA), zeolite–carbon composite (Na-P1(C)) and pure zeolite (Na-P1), were investigated. The applied solids were characterized using the following techniques: XRD, SEM-EDS, TEM, porosimetry, SLS, electrophoresis and potentiometric titration. The heavy metal concentration in the probes was determined by applying ICP-OES spectroscopy. Adsorption/desorption and electrokinetic measurements were performed in the systems containing one or two adsorbates. The obtained results indicated that Pb(II) ions are adsorbed in larger amounts on the investigated solid surface due to the molecular sieving effect. The largest adsorption capacity relative to lead(II) ions was observed for pure Na-P1 zeolite (407 mg/g). The simultaneous presence of Pb(II) + Zn(II) mixed adsorbates minimally affects the amount of adsorbed Pb(II) ions and causes a significant decrease of Zn(II) ion adsorption (in comparison with analogous systems containing single adsorbates). It was also shown that all solids can be efficiently regenerated using hydrochloric acid. Thus, the selected pure zeolite can be successfully applied in soil remediation or other purifying technologies as an effective Pb(II) adsorbent.

Keywords: Na-P1 zeolite; zeolite–carbon composite; zinc and lead adsorption; simultaneous ions removal; desorption by HCl/NaOH; electrokinetic parameters



Citation: Panek, R.; Medykowska, M.; Szewczuk-Karpisz, K.; Wiśniewska, M. Comparison of Physicochemical Properties of Fly Ash Precursor, Na-P1(C) Zeolite–Carbon Composite and Na-P1 Zeolite—Adsorption Affinity to Divalent Pb and Zn Cations. *Materials* **2021**, *14*, 3018. <https://doi.org/10.3390/ma14113018>

Academic Editor: Lijian Leng

Received: 29 April 2021

Accepted: 28 May 2021

Published: 2 June 2021

Publisher's Note: MDPI stays neutral with regard to jurisdictional claims in published maps and institutional affiliations.



Copyright: © 2021 by the authors. Licensee MDPI, Basel, Switzerland. This article is an open access article distributed under the terms and conditions of the Creative Commons Attribution (CC BY) license (<https://creativecommons.org/licenses/by/4.0/>).

1. Introduction

Human activities and their interactions with the environment, such as mining, oil and gas quarrying, have a significant impact on the progressive destruction and pollution of natural ecosystems [1]. Increased soil exploitation related to attempts to provide food for the still significantly increasing world population led to soil degradation [2,3]. Therefore, it is important to look for as many solutions as possible to minimize the results of adverse processes occurring in soil. Organic amendments, such as livestock manure, biosolids, pulp and paper mill by-products, etc. [4], have been used successfully. Biochar amendments, green waste compost and triple superphosphate (TSP) as well as clay minerals, such as kaolinite [5], were applied to reduce the bioavailability of heavy metals in soils [6,7]. Another way to improve soil quality is zeolites, which have been successfully used as an additive for the composting of organic solid waste. This allowed for a shorter composting period, a reduction in greenhouse gas and ammonia emissions, as well as a reduction in the total amount and bioavailability of heavy metals. The use of zeolite-modified compost contributed to better yields, water retention and reduced loss of nutrients [8].

Zeolites are minerals, formed during hydrothermal processes (natural zeolites) or chemical processes (synthetic zeolites). They are crystalline, porous hydrated aluminosilicates of sodium and calcium, less frequently of strontium or barium. Their special properties include not only the ion-exchange ability and significant resistance to acid and high temperature, but also the possibility of removing water from the tubules (zeolite water) without disturbing the structure of the zeolite. Other unique properties are low density, catalytic properties and a large volume of free space. Zeolites also are capable of ion and molecule sorption [9,10]. Some zeolites are present in the soils, such as the most common clinoptilolite, but also chabazite, laumontite, analcime and stilbite [11,12]. Currently, synthetic zeolites are more and more widely used materials. They are applied due to physical and chemical properties and are more uniform and predictable characteristics than natural zeolites [13].

Zeolites are widely used as soil fertilizers, being a good alternative to chemicals. Zeolite-based fertilizers have the ability to reduce the nutrient release, which contributes to better nourishment of the soil and does not pose a threat of increased nitrogen, phosphorus or potassium concentrations in surface water. Surfactant-modified zeolite was used as a fertilizer carrier that makes phosphorus release slower [14]. The addition of nanoporous zeolite also increased the nitrogen bioavailability from urea fertilizers [15]. Zeolite fertilizers can be synthesized from coal ash, which is a problematic industrial by-product [16]. In remediation of heavy-metal-contaminated soils, both natural and synthetic zeolites may be applied [17,18].

The presence of heavy metals in the environment, i.e., in waters or soils, due to their properties (toxicity, stability, possibility of accumulation or carcinogenicity) is one of the most important issues that we have to deal with. On the other hand, the presence of certain metals in a given environment may be a benefit, e.g., zinc as a representative of microelements is necessary in sufficient quantities for the growth of plants, but its excess in soil inhibits their growth, disrupting their development and metabolism [19]. Lead is absolutely toxic to plants and is not needed for their growth. It threatens the life and health of animals and humans [20]. Therefore, it is important to develop new materials enabling the removal of heavy metals from the environment. Based on the performed study, it can be stated whether selected adsorbents can be successfully used in water purification and soil remediation. Hui et al. proved that both zeolite (Na-A) and zeolite–carbon composite made from coal gangue can be useful for Cu^{2+} and rhodamine B removal from a water solution [21]. In turn, Wanyonyi et al. described the influence of zeolite pore topology and chemistry, claiming that the high diameter of pores exhibited appreciable loading of the cations [22]. Kragović et al. [23] tested natural zeolite (NZA) and zeolite modified via alginate (FRA), whereas Abdelrahman et al. [24] used rice husks and aluminum can waste to produce geopolymer–zeolite products. The studies in which the natural zeolite clinoptilolite showed a similar ability to remove heavy metals (As^{5+} , Cu^{2+} , Ni^{2+} , Pb^{2+} and Zn^{2+}) as commercially available $\gamma\text{-Al}_2\text{O}_3$ have also been reported [25]. Due to the fact that inorganic and organic substances significantly affect the structure of the electrical double layer, the influence of adsorbates on the zeta potential and surface charge of zeolites and zeolite–carbon composites should also be determined [26,27].

This paper describes the synthesis and characterization of a novel Na-P1 zeolite and its Na-P1(C) zeolite–carbon composite as adsorbents reducing the bioavailability of heavy metals (zinc and lead) to plants and animals in soil. These adsorbents were tested in single and mixed systems of heavy metal ions to understand the influences of particular adsorbates on the adsorption process. In addition, high-carbon fly ash (HiC FA) was also characterized as a substrate for the hydrothermal reaction, leading to the formation of the above adsorbents [28]. To our knowledge, for the first time, a waste-based sorbent in the form of high-carbon fly ash was used for heavy metal removal, which, due to its chemical composition, cannot be used in civil engineering (the main branch of fly ash disposal). Additionally, undoubtedly, novelty is a scale of research conducted. A semi-

technical technology line was used to synthesize both sorbents, which can ease application in industry in the near future.

2. Materials and Methods

2.1. Materials

The preparation of the materials was started by obtaining the Na-P1(C) zeolite–carbon composite. Fly ash, the starting material from the Janikowo Thermal Power Plant resulting from the conventional combustion of hard coal, was used in this procedure. Due to its electromagnetic separation, the obtained high-carbon product (HiC FA) could be used to produce a carbon–zeolite composite. The final product was created in a typical zeolitization process based on the hydrothermal reaction of fly ash with an aqueous solution of sodium hydroxide [29,30].

The Na-P1(C) material was prepared on a technological line for the synthesis of ash zeolites. At the first stage, 20 kg of high-carbon ash was mixed with 90 dm³ of 3 M NaOH solution. Then the whole mixture was stirred with a mechanical stirrer at a temperature of 90 °C for 24 h. At the final stage the obtained product was washed, rinsed and dried at 105 °C. This reaction also resulted in the production of a waste solution rich in silicon and aluminum coming from the dissolution of the ash aluminosilicate glaze and sodium coming from sodium hydroxide [31,32]. This waste was a substrate for the synthesis of the second type of material, which was pure Na-P1 zeolite without ash residue. It was prepared on a technological scale using the following steps: 40 dm³ of waste solution was mixed with 10 dm³ of 2 M aqueous NaOH solution, where 80 g of aluminum foil was dissolved. The mixture was left for 48 h at 100 °C. In the next stage, the obtained product was filtered, washed and dried at a temperature of 105 °C. The materials prepared in this way were characterized in terms of mineralogy, structure and texture.

2.2. Methods

The solids characterization was performed as follows. The phase composition of the solids was characterized by X-ray diffraction in the Panalytical XPert Pro MPD(Eindhoven, The Netherlands) apparatus with a copper lamp ($\text{CuK}\alpha = 1.54178 \text{ \AA}$). The angular range was 5–65° 2 θ with a step of 0.02° 2 θ lasting 5 s. The X'Pert Highscore software ver. 4.1 (Almelo, The Netherlands) was used to process the diffraction data. The mineral phases were identified using the PDF-2 release 2010 database formalized by JCPDS-ICDD.

The Panalytical Epsilon 3 spectrometer, equipped with an X-ray tube Rh 9 W, 50 kV, 1 mA, 4096 channel spectrum analyzer and a high-resolution semiconductor SDD detector cooled by a Peltier cell, was used to determine the elemental composition. The obtained results considered the LOI (loss of ignition).

The Malvern Mastersizer 3000 apparatus allowed the estimation of the grain size through the phenomenon of laser diffraction. The experiment was carried out in the aquatic environment in the HYDRO EV attachment.

The FEI Quanta 250 FEG scanning electron microscope equipped with an EDS attachment from the EDAX company (Mahwah, NJ, USA) allowed the morphological analysis. The experiment was carried out on the samples sprayed with a conductive carbon layer at an accelerating voltage of 15 keV.

The HR/TEM analysis of the Na-P1 sample was conducted on an electron microscope, Titan G2 60–300 kV (FEI Company, Hillsboro, OR, USA), applying an accelerating voltage of the electron beam equal to 300 kV.

The ASAP apparatus supplied by Micromeritics Instrument Corporation was used to measure textural parameters (the test was carried out using a low-temperature nitrogen adsorption/desorption isotherm in liquid nitrogen at a temperature of 77 K (−194.85 °C) in the range of relative pressures p/p_0 ranging from 1.5×10^{-7} to 0.99). In turn, the analysis of the shape of nitrogen vapor adsorption isotherms was characterized by IUPAC classification [33,34]. Samples for N₂ adsorption were prepared by degassing at 300 °C for

12 h under reduced pressure in the degassing port. Then the samples were degassed at the analytical port just before analysis for 4 h at 300 °C.

The adsorbed amount determination of heavy metal ions on the surface of HiC FA, Na-P1 and Na-P1(C) was based on a static method and the following equation (Equation (1)) [35]:

$$\Gamma = \frac{c_{ads} \cdot V}{m} \quad (1)$$

where c_{ads} —the heavy metal adsorbed concentration (the difference in the heavy metal concentration in the system before and after its adsorption), V —the suspension volume, and m —the solid weight.

The samples were prepared using 0.003 g of HiC FA, Na-P1 or Na-P1(C), which was added to the solutions containing the supporting electrolyte (0.001 M NaCl) and the selected heavy metal ions with the concentrations of 10, 50, 70, 100, 150 and 200 ppm (total volume of solution was 10 cm³). In the case of mixed adsorbate systems, the concentration of both ions was 100 ppm. The pH of all samples was set to the value of 5 using 0.1 M HCl, 0.1 M NaOH and a pH meter supplied by Beckman (Brea, CA, USA). After the adsorption process, which lasted 3 h, the solid was separated from the solution by paper filters. The time of the adsorption process was established based on the kinetics study. The concentration of ions in supernatants was determined using optical emission spectrometry with inductively coupled plasma (Thermo Scientific iCAP™ 7200 ICP-OES analyzer). Based on the obtained results, the adsorption isotherms of Zn(II) and Pb(II) on the surface of HiC FA, Na-P1 and Na-P1(C) were prepared. The experimental data were fitted to the selected theoretical models, i.e., Langmuir (Equation (2)) and Freundlich (Equation (3)) [36,37]:

$$q_e = \frac{q_m K_L C_e}{1 + K_L C_e} \quad (2)$$

$$q_e = K_F C_e^{1/n} \quad (3)$$

where K_F and K_L —the Freundlich [$\text{mg/g} (\text{mg/L})^{-1/n_F}$] and Langmuir [dm^3/mg] parameters, respectively, q_e —the equilibrium adsorption capacity [mg/g], C_e —the equilibrium liquid phase concentration [mg/dm^3], q_m —the maximum adsorption capacity in a Langmuir model [mg/g], and n —the Freundlich constant related to adsorption intensity.

The samples for **adsorption kinetics study** were prepared by adding 0.003 g of the selected adsorbent to 10 cm³ of solutions containing the supporting electrolyte (0.001 M NaCl) and heavy metal ions with a concentration of 100 ppm. Then the pH was adjusted to the value of 5 and adsorption was performed for 10, 30, 60, 90, 120 and 180 min. After that step, the solids were separated by paper filters and the concentration of heavy metal ions in supernatants was determined by the ICP-OES technique. The modeling of the results was made using the equations of pseudo-first order (Equation (4)) and pseudo-second order (Equation (5)) [38–41]:

$$\frac{dq_t}{dt} = k_2(q_e - q_t) \quad (4)$$

$$\frac{dq_t}{dt} = k_2(q_e - q_t)^2 \quad (5)$$

where q_e —the adsorbed amount at equilibrium [mg/g], q_t —the adsorbed amount after time ' t ' [mg/g], and k_1 [$1/\text{min}$] and k_2 [$\text{g/mg}\cdot\text{min}$]—the equilibrium rate constants.

Desorption measurements began with the preparation of samples containing a supporting electrolyte (0.001 M NaCl), 0.003 g of HiC FA, Na-P1 or Na-P1(C) and heavy metal ions at concentrations of 100 ppm (total volume of solution was 10 cm³). Then, the pH value was adjusted to 5 and the adsorption was carried out for 3 h. The solid was separated from the solution by paper filters and then 10 cm³ of 0.1 M HCl or NaCl was added to the separated solids. The desorption process lasted 1 h, after which the solid was separated again using paper filters and the concentration of ions in supernatants was determined

by means of ICP-OES. Desorption degree (D , %) was calculated based on the equation (Equation (6)):

$$D = \frac{C_d}{C_a} \cdot 100\% \quad (6)$$

where C_d —the amount of desorbed heavy metal ions, and C_a —the amount of absorbed heavy metal ions.

Potentiometric titration was used to determine the surface charge density (σ_0) of high-carbon fly ash, zeolite and its carbon composite, without and with adsorbates. The values of this parameter, as a function of solution pH, were calculated by the difference between the volumes of titrant added to the suspension and the supporting electrolyte solution (with a defined pH value) using the computer program “titr_v3” and the following equation (Equation (7)) [42]:

$$\sigma_0 = \frac{\Delta V_{cb} F}{mS} \quad (7)$$

where c_b —the base concentration, F —the Faraday constant, m —the solid mass in the suspension, S —the specific surface area of the solid, ΔV —the difference in the volume of base that must be added to adjust the pH of the suspension and supporting electrolyte to the specified value.

The titration set consisted of a Teflon vessel containing the solution connected to an RE 204 thermostat (Lauda), an automated microburet Dosimat 765 (Metrohm) and a computer, glass and calomel electrodes (Beckman Instruments) and a PHM 240 pH meter (Radiometer) controlling the pH values. The examined suspensions were prepared by adding 0.4 g of HiC FA, 0.4 g of Na-P1 or 0.02 g of Na-P1(C) to 50 cm³ of supporting electrolyte (0.001 M NaCl). The samples were titrated with 0.1 M NaCl solution in the pH range changing from 3 to 11. One by one, the supporting electrolyte itself, suspensions without adsorbates and suspensions with one or two adsorbates were titrated. The heavy metal ion concentration was 10 ppm.

Measurements of the **electrophoretic mobility** (u_e) were performed to determine the zeta potential (ζ) of the particles, without and with all adsorbates, using the Henry equation (Equation (8)) [43]:

$$u_e = \frac{2\varepsilon_0\varepsilon\zeta}{3\eta} f[\kappa\alpha] \quad (8)$$

where ε —the dielectric constant, ε_0 —the electric permeability of vacuum, ζ —the zeta potential, η —the solution viscosity, and $f[\kappa\alpha]$ —the Henry function.

The suspensions were prepared by adding 0.01 g of HiC FA, Na-P1 or Na-P1(C) to 200 cm³ of the supporting electrolyte solution without and with one or two heavy metal ions, and then sonicated for 3 min. Next, the solution was divided into parts, and the pH of each of them was adjusted to a specific pH value (ranging from 3 to 10). The electrophoretic mobility measurements were carried out at an ion concentration of 10 ppm using Nano ZS Zetameter (Malvern Instruments).

3. Results and Discussion

3.1. Characteristics of Adsorbents

The chemical composition of high-carbon fly ash, carbon–zeolite composite and pure zeolite is shown in Table 1.

The chemical composition of all adsorbents is dominated by silicon (29.72%, 18.05% and 49.8% for HiC FA, Na-P1(C) and Na-P1, respectively) and aluminum (14.11%, 10.07%; 18.05% for HiC FA, Na-P1(C) and Na-P1, respectively). In addition, there are negligible amounts of CaO (0.31–3.67%), Fe₂O₃ (0.51–9.12%) and Na₂O (0.61–8.11%). Fly ash and composite are also characterized by a high carbon content, ranging from 29.65% to 44.49%. Table 2 presents the distribution of individual grain fractions of all adsorbents.

Table 1. Chemical composition of adsorbents: high-carbon fly ash, zeolite–carbon composite and zeolite.

	Compounds											
	Na ₂ O	MgO	Al ₂ O ₃	SiO ₂	P ₂ O ₅	SO ₃	K ₂ O	CaO	TiO ₂	Fe ₂ O ₃	LOI	C
HiC FA	0.61	1.52	14.11	29.72	0.32	1.16	2.28	3.67	0.95	8.82	36.82	29.65
Na-P1(C)	3.77	1.19	10.07	18.05	0.04	0.53	0.42	2.17	0.91	9.12	53.73	44.49
Na-P1	8.11	nd *	18.05	49.38	nd *	nd *	5.57	0.31	0.06	0.51	17.37	nd *

nd *—not detected.

Table 2. Percentage distribution of individual grain fractions (μm) of HiC FA, Na-P1 and Na-P1(C).

Fraction [μm]	HiC FA	Na-P1 [%]	Na-P1(C)
0.01–2	0.18	2.57	3.16
2–20	13.69	25.23	25.28
20–50	27.02	39.56	24.65
50–100	28.64	13.29	28.41
100–250	26.41	8.34	18.34
250–500	4.05	7.34	0.17
500–1000	0	3.64	0
1000–2000	0	0.04	0

One clearly dominant fraction was not observed in high-carbon fly ash, whereas the three main fractions 20–50, 50–100 and 100–250 μm , amounting to 27.0, 28.6 and 26.4%, respectively, were noted. The remaining fractions (equal to over 17%) are 2–20 μm (13.7%) and 250–500 μm (4.1%). The Na-P1 material is dominated by the 20–50 μm fraction, the volume content of which is 39.6%. The second is the 2–20 μm fraction (25.2%). The total volume of the particles from the particle size range of 2–100 μm is 78.1%. Obviously, particles with a diameter greater than 500 μm (3.6%) appear, which is most likely due to the fact that particles with smaller diameters agglomerate. This is typical for this type of material. In the case of the Na-P1(C) material, the total content of the 2–100 μm fraction is 78.3%, which is almost the same as for Na-P1 zeolite. However, in this case fractions 2–20, 20–50 and 50–100 μm are distributed almost evenly (25.3%, 24.7% and 28.4%, respectively) and thus, similarly to fly ash, it is difficult to unambiguously indicate the most dominant one. Additionally, the presence of particles with a diameter of 100–250 μm (18.3%) is observed, which is probably the result of the deposition of single zeolite particles on the carbon fragments, naturally increasing their size.

Figure 1 presents the curves of particle size distribution obtained for the examined adsorbents.

The particle size distribution curve obtained for the HiC FA fly ash was monomodal with a very wide peak with a maximum diameter of about 80 μm and height equal to 6.8%. The particle size distribution curves for Na-P1 and Na-P1(C) were bimodal, with easily noticeable differences in peak maxima. In the case of Na-P1, a clear maximum was observed for particles with a diameter of approx. 30 μm and a height of about 7.5%. The second maximum was noted for particles with a diameter of 400 μm (1.8%). This is consistent with the observations made for individual fractions. In contrast, for the Na-P1(C) material, the maximum of the main peak was observed for particles with a diameter of about 70 μm . This peak was about 6.8%. Importantly, the peak maximum coincides perfectly with the one observed for the HiC FA fly ash (the raw material from which Na-P1(C) was obtained). The maximum of the smaller peak was near particles with a diameter of 2.5 μm . It was 1.8%, similarly to Na-P1. It can also be observed that the main peak is broad and not symmetrical, so that the smaller peak is not perfectly separated. Again, this perfectly reflects the fraction-specific observation indicating the absence of a dominant fraction (very broad main peak).

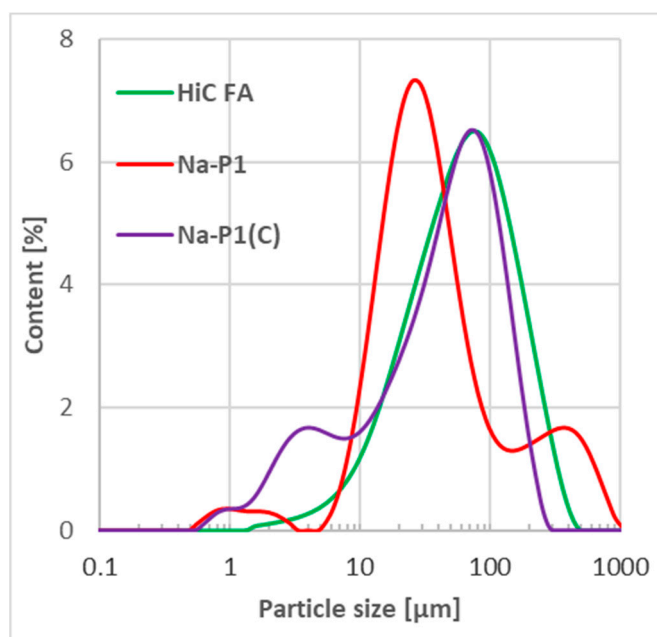


Figure 1. Particle size distribution of HiC FA, Na-P1 and Na-P1(C).

Morphological analyses of high-carbon fly ash are presented in Figure 2. Figure 3 shows the morphology of the Na-P1(C), whereas Figure 4, that of Na-P1.

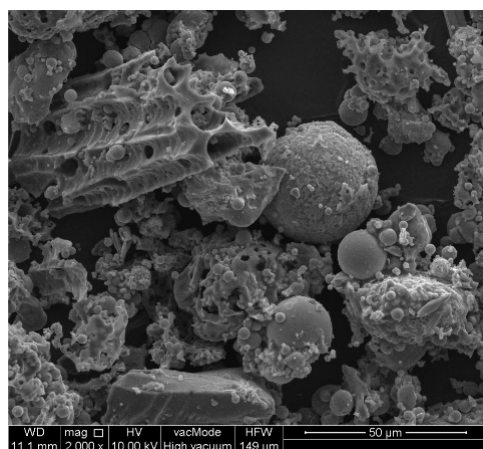


Figure 2. Morphological analyses of HiC FA.

SEM micrographs of HiC FA show spherical structures of aluminosilicate glaze, irregular forms of quartz and mullite, unburned carbon fragments and carbon sinters with embedded aluminosilicate glaze spheres. In the SEM micrographs of Na-P1(C), zeolite crystals are very well formed, creating lamellar aggregates with diameters ranging from 2 to 5 μm. These crystals are formed in the carbon ash zone as well as on fragments of aluminosilicate glaze. They have the characteristics of single clusters or mutually overgrown aggregates. Figure 3 shows the chemical analysis performed using EDS on the zeolite crystal (point 1) and the carbon fragment (point 2). In the first case, the dominant elements were aluminum, silicon, sodium, magnesium and oxygen, which are part of the zeolite, whereas in the second case, chemical analysis showed the presence of unburned carbon on which zeolite crystals were formed. In addition, some part of the carbon in the sample also came from its preparation (carbon sputtering). As was mentioned above, Figure 4 shows the morphology of pure Na-P1 zeolite (with no ash residue). The zeolite crystals are very well formed, ranging in size from 6 μm to 12 μm. This picture also shows the EDS analysis performed on zeolite crystals (points 1 and 2). In both cases, the dominant elements were

silicon, aluminum, sodium and oxygen, and small amounts of calcium, potassium and magnesium. The presence of carbon was associated with the sample preparation. To obtain more information about the Na-P1 structure, HR/STEM images were taken (Figure 5a,b).

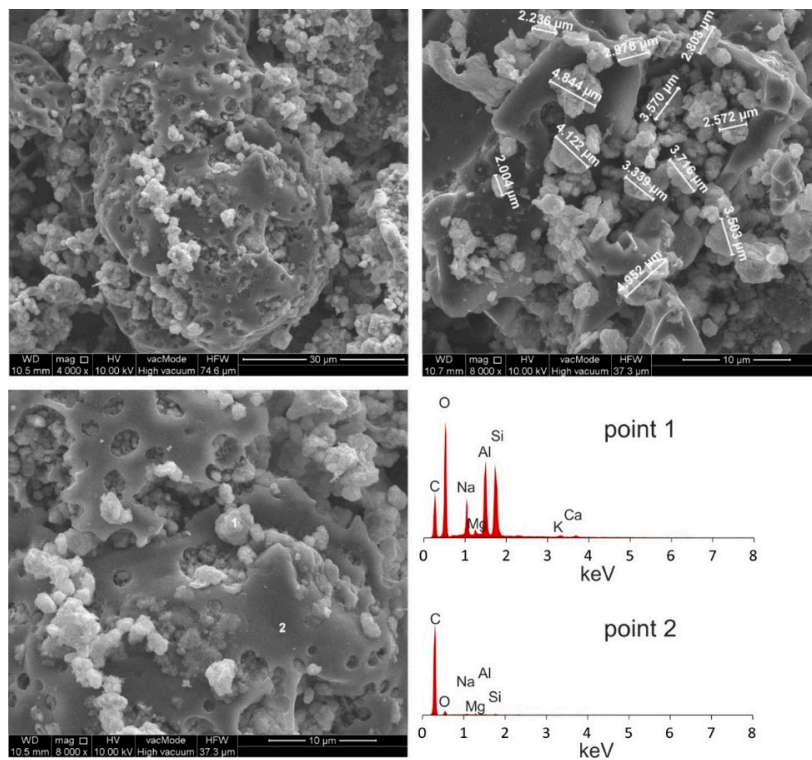


Figure 3. Morphological analyses of Na-P1(C).

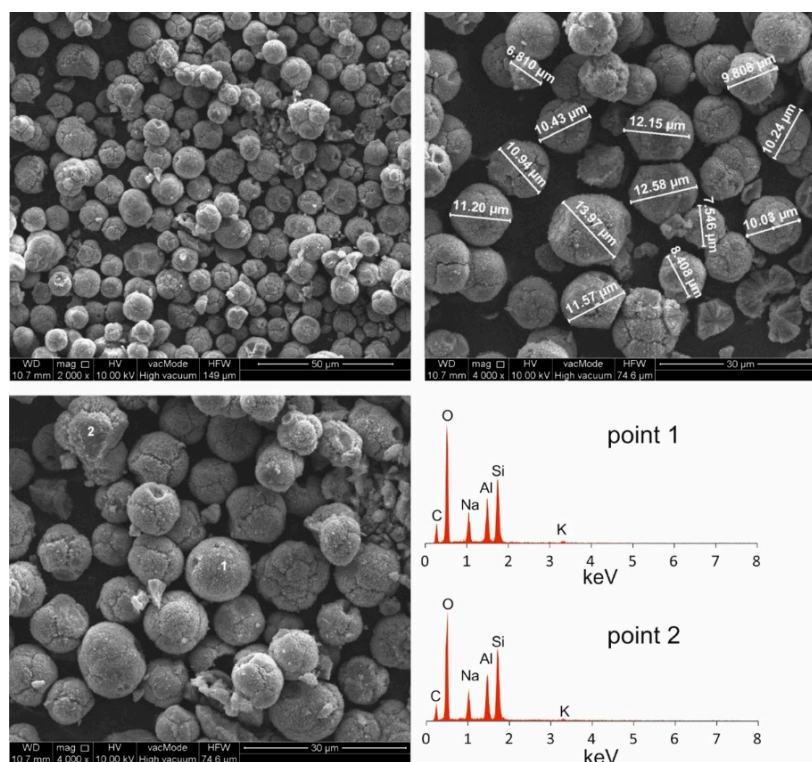


Figure 4. Morphological analyses of Na-P1.

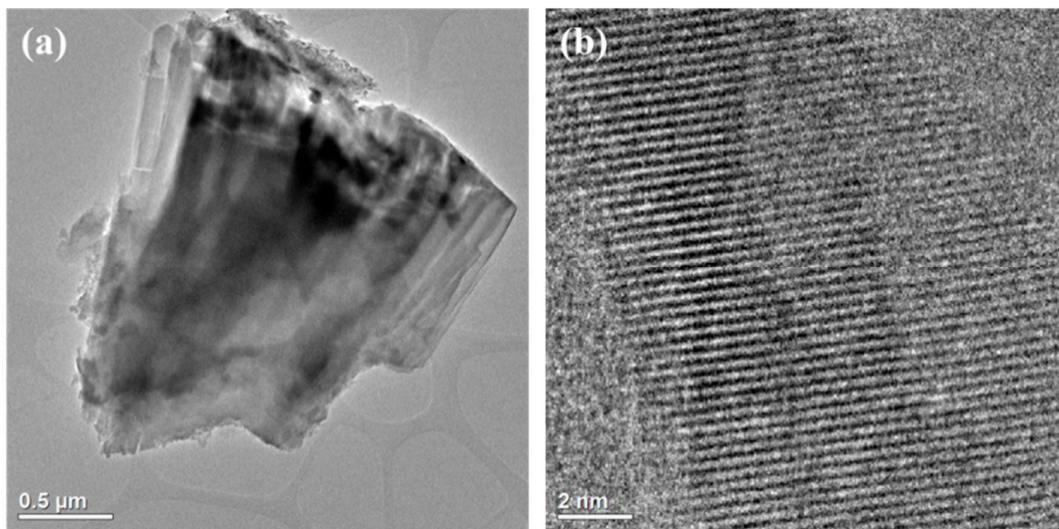


Figure 5. HR/TEM images of Na-P1: whole crystal (a), cross-section with channels (b).

Figure 5a shows a fragment of a larger zeolite aggregate about 5 μm in size. On the other hand, Figure 5b shows a cross section of the zeolite crystal. In the microarea, one can observe pores as brighter places and their walls as darker ones. The structure of the analyzed material is characterized by well-ordered, cylindrical and regular micropores.

Diffractograms of the phase composition of high-carbon fly ash, Na-P1(C) composite and pure Na-P1 zeolite are shown in Figure 6.

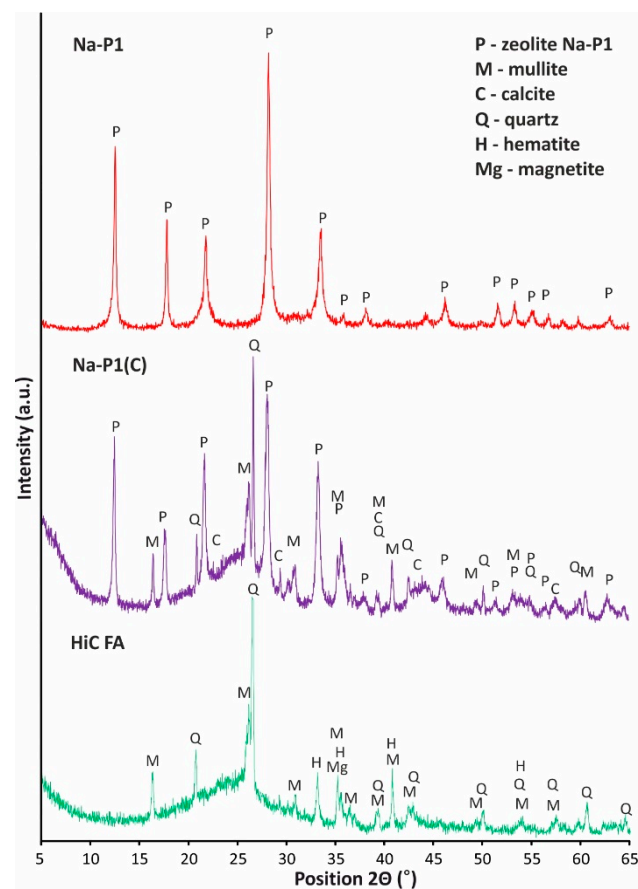


Figure 6. Phase analysis of high-carbon fly ash, zeolite–carbon composite Na-P1(C) and zeolite Na-P1 samples.

The fly ash mineral composition is dominated by amorphous aluminosilicate glaze, the presence of which is shown in the graph in the form of a raised background in the angle range 2Θ from 15 degrees to 35 degrees. The main crystalline component is mullite, recognized by the strongest reflections of interplanar distances $d_{hkl} = 5.38; 3.41; 2.89; 2.66 \text{ \AA}$. A secondary mineral component in the tested ash is quartz, recognized by the strongest reflections $d_{hkl} = 4.26; 3.34; 2.45; 2.28; 1.81 \text{ \AA}$. Moreover, the phase composition of fly ash is complemented by iron oxides in the form of hematite and magnetite, which were recognized by the strongest reflections $d_{hkl} = 3.68; 2.29; 2.21; 1.6 \text{ \AA}$. The diffractograms of the Na-P1(C) and the Na-P1 zeolite indicate that only the pure Na-P1 zeolite sample obtained from the filtrate has a monomineral character. The presence of the zeolite phase was characterized by the following reflections: $d_{hkl} = 7.21; 5.05; 4.11; 3.20; 2.91; 2.69; 2.53; 2.38; 1.97 \text{ \AA}$. The composite sample also contains phases related to unreacted ash residue in the form of aluminosilicate glaze, mullite ($d_{hkl} = 5.38; 3.40; 2.79; 2.59 \text{ \AA}$), quartz ($d_{hkl} = 4.25; 3.34; 2.45; 2.28 \text{ \AA}$) and calcite ($d_{hkl} = 3.03; 2.49; 2.09; 1.88 \text{ \AA}$).

Textural parameters (S_{BET} —specific surface area, S_{micro} —micropore area, V_t —total pore volume, V_{micro} —micropore volume, and D —average pore diameter) of high-carbon fly ash, zeolite and zeolite–carbon composite are presented in Table 3.

Table 3. Textural parameters of HiC FA, Na-P1 and Na-P1(C) adsorbents.

Adsorbent	S_{BET} [m ² /g]	S_{micro} [m ² /g]	V_t [cm ³ /g]	V_{micro} [cm ³ /g]	D (4 V/A) [nm]
HiC FA	46.19	10.72	0.064	0.0060	5.66
Na-P1	26.71	4.30	0.05	0.0017	6.93
Na-P1(C)	69.85	16.90	0.12	0.0070	6.75

These results indicated that all adsorbents had a poorly developed surface. They contained mesopores of average diameter in the range 5.66–6.93 nm. Figure 7 shows the nitrogen adsorption–desorption isotherms at liquid nitrogen temperature of the studied materials. It can be observed that the Na-P1(C) material is characterized by the highest nitrogen adsorption, which is confirmed by the textural parameters of these materials presented in Table 3.

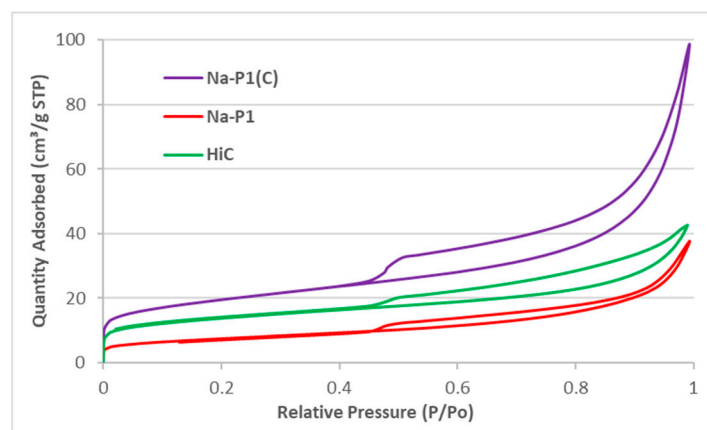


Figure 7. N₂ adsorption/desorption isotherms of the studied materials.

3.2. Adsorption Capacity of HiC FA, Zeolite–Carbon Composite and Pure Zeolite Relative to Zn(II)/Pb(II) Ions in the Single Adsorbate Systems

Figure 8a–d show the adsorption kinetics and isotherms of Pb(II) and Zn(II) ions on the HiC FA, zeolite and zeolite–carbon composite surfaces, whereas in Table 4 the kinetics and isotherm parameters are presented.

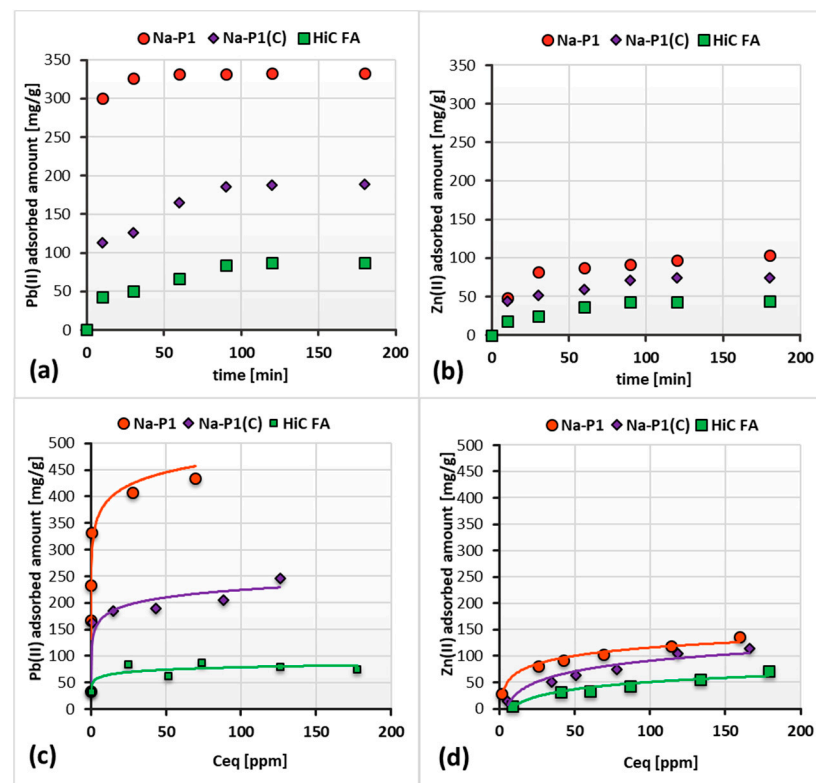


Figure 8. Adsorption kinetics isotherms of Pb(II) (a,c) and Zn(II) ions (b,d) on the HiC FA, Na-P1 and Na-P1(C) surfaces in the single systems at pH 5.

Table 4. Kinetics and isotherm parameters of Pb(II) and Zn(II) adsorption on the HiC FA, Na-P1 and Na-P1(C) surfaces at pH 5.

System		Pseudo-Second-Order Model		
		q_e [mg/g]	k_2 [g/(mg·min)]	R^2
Pb(II)	Na-P1	322.581	0.0004	0.997
	Na-P1(C)	212.766	0.0004	0.997
	HCFA	129.870	0.0001	0.959
Zn(II)	Na-P1	32.362	0.0023	0.996
	Na-P1(C)	30.030	0.0019	0.998
	HCFA	19.083	0.0011	0.940
System		Langmuir model		
		q_m [mg/g]	K_L [dm ³ /mg]	R^2
Pb(II)	Na-P1	432.572	3.755	0.999
	Na-P1(C)	236.661	0.248	0.978
	HCFA	76.548	2.911	0.988
Zn(II)	Na-P1	144.062	0.053	0.980
	Na-P1(C)	156.988	0.014	0.962
	HCFA	142.192	0.007	0.860

The performed measurements allowed us to determine the time after which the amount of adsorbate on the solid surface did not change. As can be seen in Figure 8a,b, this time for the fly ash, zeolite and composite differs. Among the systems containing Pb(II) ions, the equilibrium was established the fastest in the case of Na-P1, i.e., after 30 min. For Na-P1(C) and HiC FA, this time was equal to 60 min. On the other hand, among the system

containing Zn(II) ions, the equilibrium was reached after 120 min in all the studied systems. Thus, it can be concluded that in systems containing Pb(II) ions, the time required to reach equilibrium is shorter than in the case of systems containing Zn(II) ions.

The observed adsorption capacities varied between selected solids, as can be seen in Figure 8c,d. Pb(II) cations are apparently better absorbed on fly ash, zeolite and its carbon composite than Zn(II) cations. The adsorbed amount of Pb(II) on the Na-P1 exceeds twice the adsorbed amount of this element on the Na-P1(C) surface, and 2.5 times the adsorbed amount on the HiC FA one. For an initial Pb(II) concentration of 150 ppm, the amount of adsorbed heavy metal is 407.34 mg/g for Na-P1, 205.00 mg/g for Na-P1(C) and 78.67 mg/g for HiC FA. Zn(II) is absorbed less efficiently. The difference in adsorption level between Zn(II) and Pb(II) cations is best seen in the case of Na-P1, where the amount of the adsorbed Pb(II) is 3.5 times larger than Zn(II). For an initial Pb(II) concentration of 150 ppm, the amount of adsorbed Pb(II) ions is 407.34 mg/g, whereas the amount of adsorbed Zn(II) ions is 119.33 mg/g. The significantly higher adsorption of Pb(II), compared to Zn(II), can be explained by the different affinity of these ions for zeolite, which is the result of various radii and energies of hydration of these ions. The molecular sieve effect, which is characteristic of systems containing synthetic zeolites, can explain this phenomenon. It assumes that the smaller the radius of the hydrated cation and the higher its hydration energy are, the more difficult ion penetration into the zeolite pores is. As a result, the participation of the cation in ion exchange is prevented. In the systems studied, Pb(II) has a much larger radius of the hydrated ion, which simplifies its diffusion into the pores of the zeolite and effective ion exchange with, e.g., Mg and Ca cations. As a result, a considerable increase in Pb(II) adsorption is observed [44,45].

The experimental kinetics parameters were better fitted to the pseudo-second-order model. This model assumes that the rate-controlling step is a chemical reaction—exchange or sharing of electrons between heavy metal ions and adsorbents, resulting in the formation of chemical bonds (covalent or ionic) between them. So, the Zn(II) and Pb(II) adsorption involved chemisorption. The good fit is indicated by the value of the squared correlation coefficient R^2 , shown in Table 4 [46]. Analysis of theoretical and experimental data led to the conclusion that the adsorption of both heavy metal ions is slightly better fitted to the Langmuir model than to the Freundlich one. Thus, in the systems, a monolayer of uniform energy is formed [47,48].

3.3. Adsorption Capacity of HiC FA, Zeolite and Its Carbon Composite Relative to Zn(II) and Pb(II) Ions in the Mixed Adsorbate Solutions

Figure 9a,b show adsorption kinetics of Zn(II) and Pb(II) ions on the HiC FA, Na-P1, Na-P1(C) surfaces in systems containing both ions simultaneously. In turn, Figure 10a,b present a comparison of the adsorbed amount of Pb(II) or/and Zn(II) on the high-carbon fly ash, zeolite and zeolite–carbon composite surfaces in the single and mixed systems.

The analysis of the obtained results showed that the simultaneous presence of Pb(II) and Zn(II) ions did not significantly affect the time of establishing the adsorption equilibrium in the studied systems. Furthermore, the amount of adsorbed Pb(II) ions on the HiC FA, Na-P1, Na-P1(C) surfaces did not change significantly since Zn(II) ions were added to the system. On the other hand, in the case of Zn(II) adsorption, the addition of Pb(II) ions to the system resulted in approximately a threefold decrease in the adsorbed amount of zinc. The reduced amount of zinc adsorbed in the mixed systems compared to the single ones may be caused by competition for adsorbents' active sites and the aforementioned effect, resulting in a higher affinity of Pb(II) ions for three-dimensional zeolite structures.

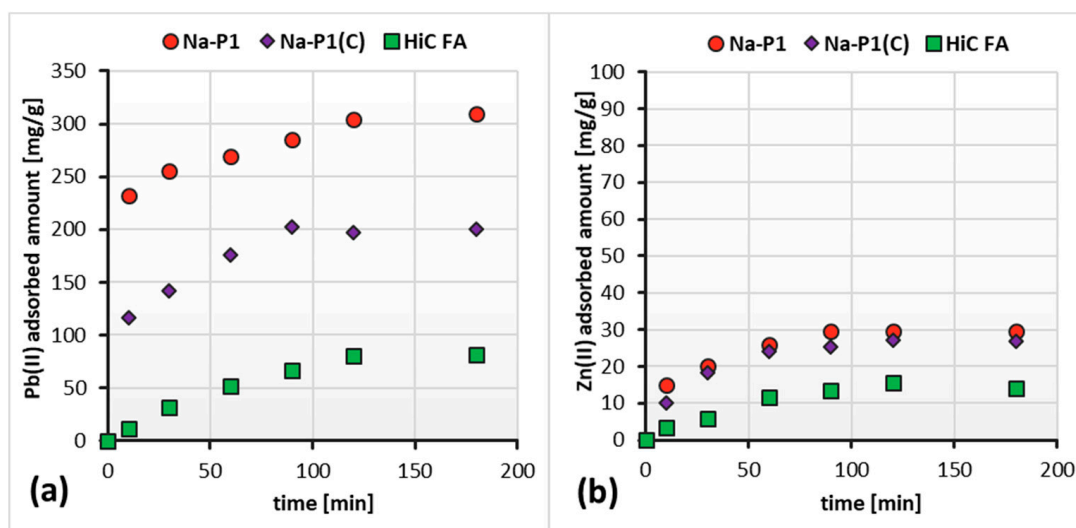


Figure 9. Adsorbed amounts of Pb(II) (a) and Zn(II) (b) on the HiC FA, Na-P1 and Na-P1(C) surfaces in the mixed systems as a function of time, at pH 5.

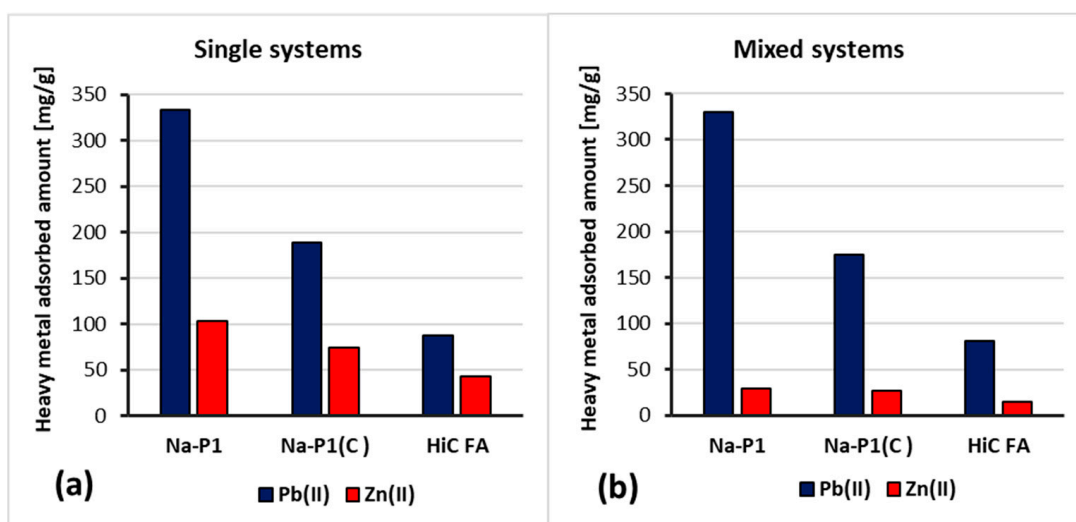


Figure 10. Amounts of Pb(II) and Zn(II) ions adsorbed on HCFA, Na-P1 and Na-P1(C) in the single (a) and mixed (b) systems at pH 5.

3.4. Changes in Surface Charge Density of HiC FA, Na-P1 and Na-P1(C) Particles as a Result of Zn(II) and/or Pb(II) Adsorption

Figure 11a–c show changes in surface charge density of the HiC FA, Na-P1 and Na-P1(C) solids as a function of solution pH, depending on the added adsorbate. In turn, Table 5 shows the changes in the pH_{pzc} (pzc —point of zero charge) values of the adsorbent particle in the examined systems of adsorbates.

As it results from the presented potentiometric titration curves, at the pH value of 5, i.e., under the conditions in which the adsorption study was conducted, the surfaces of the all adsorbents assumed a positive charge. The point of zero charge indicated the pH value at which the charge of the solid surface equals zero. At a pH higher than the pH_{pzc} of the solid, its surface takes a negative charge, and correspondingly, at a pH lower than the pH_{pzc} , the surface of the solid becomes a positive charge [49]. Despite the unfavorable electrostatic repulsion at pH 5, adsorption of cations occurs on positively charged solids due to the unique structure of zeolites. They can boast a three-dimensional system of channels and chambers of strictly defined molecular dimensions, which gives zeolites the properties of molecular sieves and enables the occurrence of ion exchange. Moreover, as

proved by kinetics studies, chemical bonds between simple metal ions and the solid surface are formed [50–53].

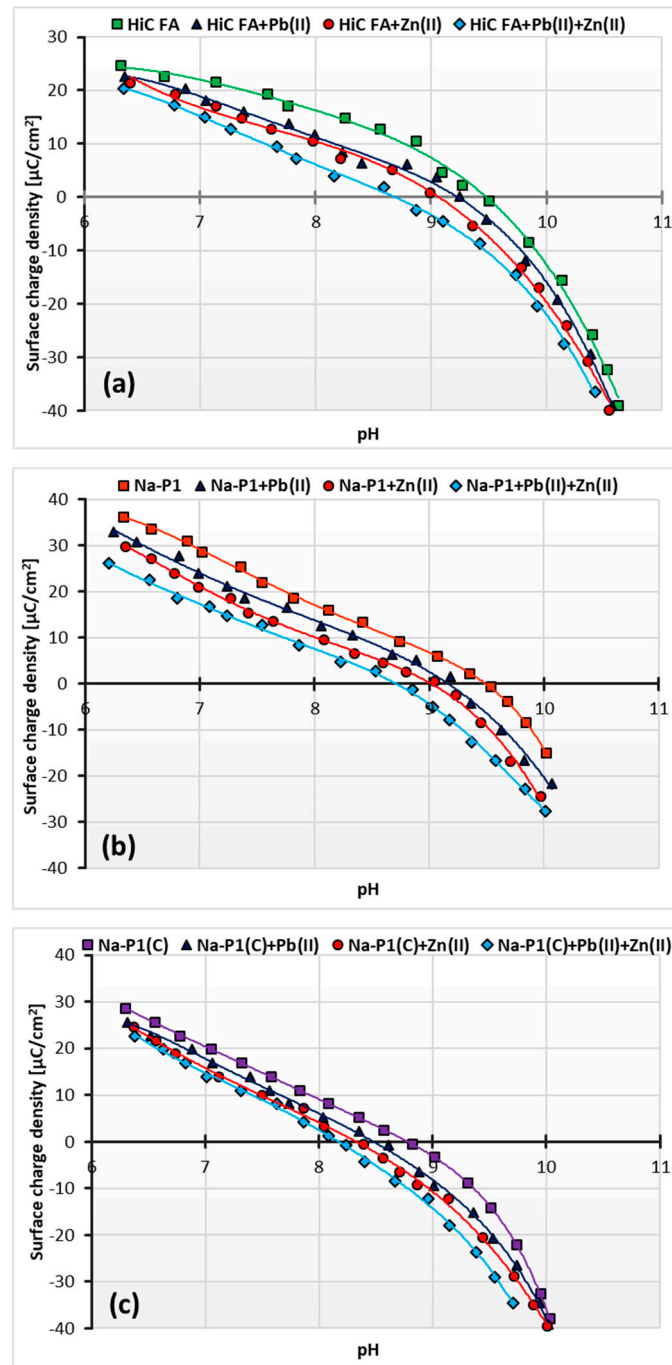
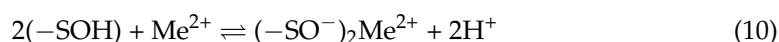
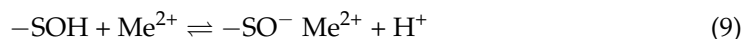


Figure 11. Surface charge density of HiC FA (a), Na-P1 (b) and Na-P1(C) (c) without and with one or two heavy metal ions.

Table 5. Comparison of the pH_{pzc} values of HiC FA, Na-P1, Na-P1(C) particles in the absence or presence of heavy metal ion/ions.

Solid	Na-P1	Na-P1(C)	HiC FA
Without adsorbates	9.6	8.8	9.5
With Pb(II)	9.1	8.5	9.2
With Zn(II)	9.0	8.4	9.0
With Pb(II) + Zn(II)	8.6	8.3	8.6

The point of zero charge is 9.5 for HiC FA, 9.6 for Na-P1, and 8.8 for Na-P1(C). For all adsorbents, this parameter decreases after adding Pb(II) ions, respectively, to 9.2 for HiC FA, 9.1 for Na-P1 and 8.5 for Na-P1(C) and after the addition of Zn^{2+} ions to 9 for HiC FA and Na-P1, and to 8.4 for Na-P1(C). Moreover, in a system containing both heavy metal ions, pH_{pzc} decreases most noticeably, for HiC FA and Na-P1 to 8.6, and for Na-P1(C) to 8.3. This means that the adsorption of heavy metal ions affects the surface charge of the adsorbents, causing the pH_{pzc} to shift towards lower values, which is a commonly observed phenomenon. Adsorption of small ions (cations in this case) creates oppositely charged sites on the surface of the adsorbent. It manifests itself in a decrease of the solid surface charge density and, consequently, in a shift of pH_{pzc} position towards smaller pH values. Such a phenomenon may be described by the following equations (Equations (9)–(11)) [54,55]:



where Me is a Pb or Zn atom.

3.5. Changes in Zeta Potential of HiC FA, Na-P1 and Na-P1(C) Particles as a Result of Zn(II) and/or Pb(II) Adsorption

Figure 12a–c presents the changes in zeta potential of adsorbents ions as a function of solution pH, depending on the added ions, whereas Table 6 shows the changes in pH_{iep} (iep—isoelectric point) values of the adsorbent particles, depending on the composition of the studied system.

Table 6. Comparison of the pH_{iep} values of the HiC FA, Na-P1, Na-P1(C) particles in the absence or presence of heavy metal ion/ions.

Solid	Na-P1	Na-P1(C)	HiC FA
Without adsorbates	-	4.0	-
With Pb(II)	-	3.2	3.2
With Zn(II)	-	-	-
With Pb(II) + Zn(II)	-	-	3.0

The pH at which the charge of a slipping plane area is equal to zero is called the isoelectric point (pH_{iep}). This plane is the interface separating the stiff part of the liquid “attached” to the surface of the solid (specifically and electrostatically bound water, ions and hydrated ions) from the diffuse part of the solution. Whether the pH_{iep} takes on positive or negative values is determined by the predominance of ions carrying a positive or negative charge in this plane. At pH values higher than the solid pH_{iep} , the zeta potential becomes positive values, and at pH values lower than pH_{iep} , negative ones [56,57].

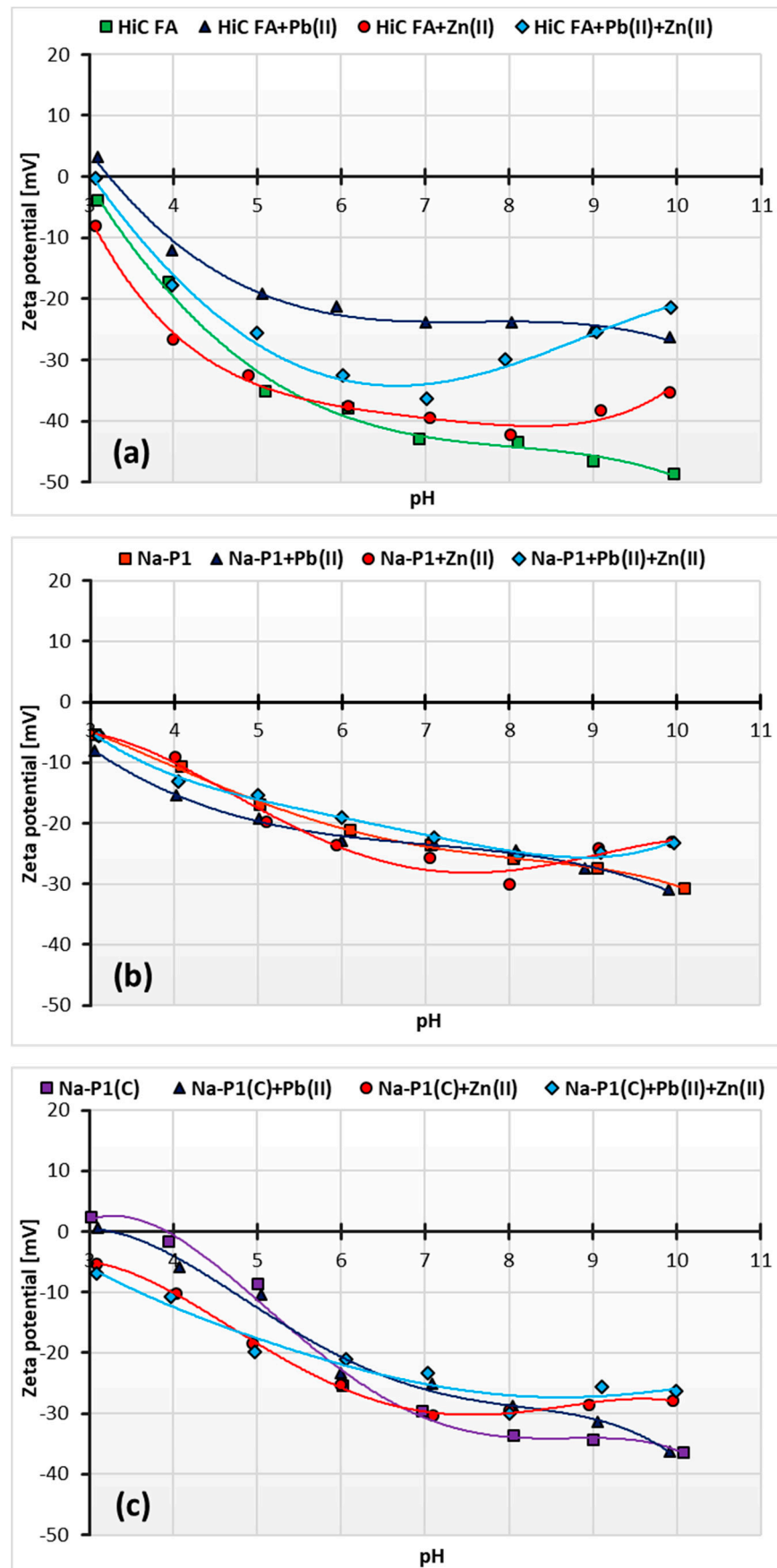


Figure 12. Zeta potential of the HiC FA 9 (a), Na-P1 (b) and Na-P1(C) (c) without and with one or two heavy metal ions.

The pH_{iep} values of the adsorbent particles in the studied systems are not in the range of the tested pH values. This indicates that pH_{iep} is below the value of 3. This applies, for example, to systems with Na-P1, both without adsorbates and with one or two adsorbates, as well as to Na-P1(C) (in systems with Zn(II) ions and Pb(II) and Zn(II) simultaneously) and HiC FA (without adsorbates and with Zn(II) ions). The isoelectric point of Na-P1(C) is located at pH about 4 and decreases to the value 3.2 with the addition of Pb(II) ions. For suspensions containing HiC FA, the most significant decrease in zeta potential is observed. It is manifested by a change in pH_{iep} value from 3.2 for the system with Pb(II) ions to 3 for the system with Zn(II) and Pb(II) ions.

The specific increase in the zeta potential at pH values in the range 8–10 can be described by the effect of charge reversal, which occurs especially in the systems with Zn(II) ions. The charges of counterions in the inner part of the electrical double layer exceed the charge of ions on the solid surface, resulting in the same charge on the outer part and on the surface. The effect caused by Zn(II) ion adsorption is also called overcharging or overloading of the electrical double layer [57].

3.6. Desorption Degree of Zn(II) and Pb(II) from HiC FA, Na-P1 and Na-P1(C) Surfaces

Figure 13a,b presents desorption degrees for the studied adsorbents.

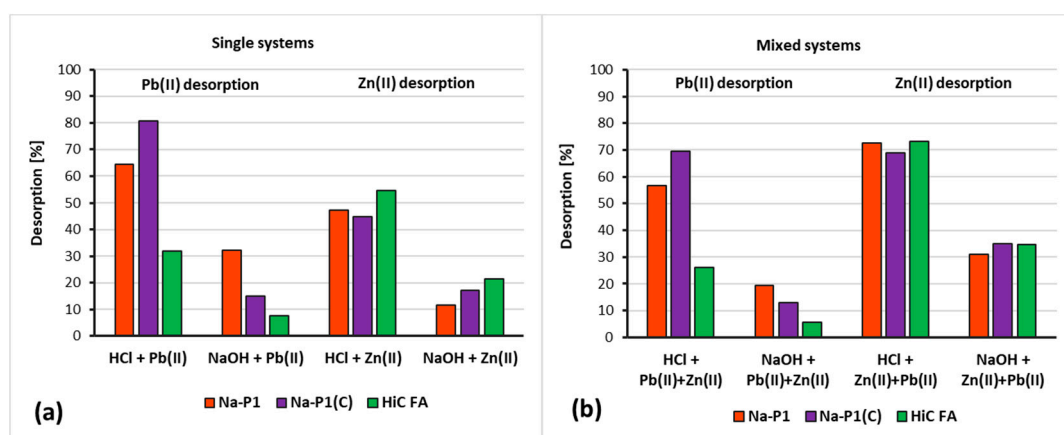


Figure 13. Desorption (%) of Zn(II) and Pb(II) ions from the HiC FA, Na-P1 and Na-P1(C) surfaces in single (a) and mixed (b) systems using 0.1 M HCl or 0.1 M NaOH.

The analysis of the data presented in Figure 13 leads to the conclusion that hydrochloric acid is a better desorbing agent than sodium base. This trend is present in all suspensions studied, both for single and mixed systems, regardless of the adsorbate or adsorbent used. The most efficient desorption from the surface of zeolite and zeolite–carbon composite in single systems took place with Pb(II) ions, whereas the greatest desorption from HiC FA surface occurred in systems containing Zn(II) ions. In mixed systems, these trends were similar.

4. Conclusions

Two types of sorbents were obtained from the waste that is fly ash—a zeolite–carbon composite and pure zeolite. Both zeolite and its carbon composite showed significantly better adsorption capacities than their precursor, fly ash. This is a result of their better textural and morphological parameters obtained due to the conversion of fly ash (zeolite–carbon composite) and waste solution (pure zeolite). Pb(II) ions were adsorbed more efficiently than Zn(II) ones and their adsorption occurs fast. The largest adsorption takes place on the Na-P1 surface (407.34 mg/g for Pb(II)), whereas the smallest on the HiC FA one (78.67 mg/g for Pb(II)). Bounding of all adsorbates occurs through chemisorption and ion adsorption following the Langmuir model. In mixed systems, Pb(II) ions adsorb more efficiently due to the molecular sieving effect. In the mixed systems of adsorbates, the

presence of Zn(II) ions minimally influences the adsorbed amount of Pb(II) ions. On the contrary, the addition of Pb(II) ions to the system results in a threefold decrease in the adsorbed amount of Zn(II) ions. The addition of divalent heavy metal cations decreases the pH_{pzc} . More efficient desorption of heavy metal ions (reaching 80%) occurs with the use of hydrochloric acid (in comparison with sodium base). Both the composite and pure zeolite, due to the method of their synthesis, may be an alternative to commercial sorbents in terms of heavy metal ion removal from aqueous solutions. Such use of fly ash is in line with the current ecological trends.

Author Contributions: Conceptualization, R.P.; methodology, M.M., K.S.-K., M.W. and R.P.; software, M.M. and R.P.; validation, K.S.-K., R.P. and M.W.; formal analysis, R.P. and M.W.; investigation, M.M., K.S.-K., M.W. and R.P.; resources, R.P.; data curation, M.W. and R.P.; writing—original draft preparation, M.M., K.S.-K. and R.P.; writing—review and editing, M.M., K.S.-K. and M.W.; visualization, R.P. and M.M.; supervision, M.W. and R.P.; project administration, R.P.; funding acquisition, R.P. All authors have read and agreed to the published version of the manuscript.

Funding: This work was financed by the National Centre for Research and Development project Lider contract number LIDER/19/0072/L-9/17/NCBR/2018.

Institutional Review Board Statement: Not applicable.

Informed Consent Statement: Not applicable.

Data Availability Statement: The data presented in this study are available on request from the corresponding author.

Acknowledgments: We would like to thank Wojciech Franus for his scientific support.

Conflicts of Interest: The authors declare no conflict of interest.

References

- Liu, X.B.; Zhang, X.Y.; Wang, Y.X.; Sui, Y.Y.; Zhang, S.L.; Herbert, S.J.; Ding, G. Soil degradation: A problem threatening the sustainable development of agriculture in Northeast China. *Plant Soil Environ.* **2010**, *56*, 87–97. [[CrossRef](#)]
- Domagała-Świątkiewicz, I. The impact of agricultural activity on the natural environment. Environmental protection in the 21st century. In *New Challenges and Threats*; red. K. Wiecha i inni, Fundacja Na Rzecz Wspierania Badań Naukowych: Kraków, Poland, 2005; pp. 57–71. (In Polish)
- Louwagie, G.; Gay, S.H.; Sammeth, F.; Ratering, T. The potential of European Union policies to address soil degradation in agriculture. *Land Degrad. Dev.* **2010**, *22*, 5–17. [[CrossRef](#)]
- Larney, F.J.; Angers, D.A. The role of organic amendments in soil reclamation: A review. *Can. J. Soil Sci.* **2012**, *92*, 19–38. [[CrossRef](#)]
- Szewczuk-Karpisz, K.; Tomczyk, A.; Komaniecka, I.; Choma, A.; Adamczuk, A.; Sofińska-Chmiel, W. Impact of *Sinorhizobium meliloti* Exopolysaccharide on Adsorption and Aggregation in the Copper(II) Ions/Supporting Electrolyte/Kaolinite System. *Materials* **2021**, *14*, 1950. [[CrossRef](#)] [[PubMed](#)]
- Karami, N.; Clemente, R.; Moreno-Jiménez, E.; Lepp, N.W.; Beesley, L. Efficiency of green waste compost and biochar soil amendments for reducing lead and copper mobility and uptake to ryegrass. *J. Hazard. Mater.* **2011**, *191*, 41–48. [[CrossRef](#)]
- Wang, R.; Shafi, M.; Ma, J.; Zhong, B.; Guo, J.; Hu, X.; Xu, W.; Yang, Y.; Ruan, Z.; Wang, Y.; et al. Effect of amendments on contaminated soil of multiple heavy metals and accumulation of heavy metals in plants. *Environ. Sci. Pollut. Res.* **2018**, *25*, 28695–28704. [[CrossRef](#)]
- Soudejani, H.T.; Kazemian, H.; Inglezakis, V.J.; Zorpas, A.A. Application of zeolites in organic waste composting: A review. *Biocatal. Agric. Biotechnol.* **2019**, *22*, 101396. [[CrossRef](#)]
- Gottardi, G.; Galli, E. *Natural Zeolites*; Springer: Berlin/Heidelberg, Germany, 1985; pp. 1–34.
- Inglezakis, V.J.; Zorpas, A.A. *Handbook of Natural Zeolites*; Bentham Science: Sharjah, United Arab Emirates, 2012; pp. 3–133.
- Ming, D.W.; Boettinger, J.L. Zeolites in Soil Environments. *Rev. Miner. Geochem.* **2001**, *45*, 323–345. [[CrossRef](#)]
- Hay, R.L.; Sheppard, R.A. Occurrence of Zeolites in Sedimentary Rocks: An Overview. *Rev. Miner. Geochem.* **2001**, *45*, 217–234. [[CrossRef](#)]
- Król, M. Natural vs. Synthetic Zeolites. *Crystals* **2020**, *10*, 622. [[CrossRef](#)]
- Bansiwal, A.K.; Rayalu, S.S.; Labhasetwar, N.K.; Juwarkar, A.A.; Devotta, S. Surfactant-Modified Zeolite as a Slow Release Fertilizer for Phosphorus. *J. Agric. Food Chem.* **2006**, *54*, 4773–4779. [[CrossRef](#)]
- Manikandan, A.; Subramanian, K.S. Fabrication and characterization of nanoporous zeolite based N fertilizer. *Afr. J. Agric. Res.* **2014**, *9*, 276–284.
- Flores, C.G.; Schneider, H.; Marcilio, N.R.; Ferret, L.; Oliveira, J.C.P. Potassic zeolites from Brazilian coal ash for use as a fertilizer in agriculture. *Waste Manage.* **2017**, *70*, 263–271. [[CrossRef](#)] [[PubMed](#)]

17. Shi, W.; Shao, H.; Li, H.; Shao, M.; Du, S. Progress in the remediation of hazardous heavy metal-polluted soils by natural zeolite. *J. Hazard. Mater.* **2009**, *170*, 1–6. [[CrossRef](#)] [[PubMed](#)]
18. Hudcová, B.; Osacký, M.; Vítková, M.; Mitzia, A.; Komáreka, M. Investigation of zinc binding properties onto natural and synthetic zeolites: Implications for soil remediation. *Micropor. Mesopor. Mat.* **2021**, *317*, 111022. [[CrossRef](#)]
19. Moynier, F.; Pichat, S.; Pons, M.-L.; Fike, D.; Balter, V.; Albarède, F. Isotopic fractionation and transport mechanisms of Zn in plants. *Chem. Geol.* **2009**, *267*, 125–130. [[CrossRef](#)]
20. Liu, J.; Dong, Y.; Xu, H.; Wang, D.; Xu, J. Accumulation of Cd, Pb and Zn by 19 wetland plant species in constructed wetland. *Hazard. Mater.* **2007**, *147*, 947–953. [[CrossRef](#)]
21. Hui, L.; Feng, Z.; Jing, W.; Jianmin, Z.; Xiaohui, H.; Lai, C.; Pengfei, H.; Jian-ming, G.; Qiang, Z.; Sajid, B.; et al. Facile preparation of zeolite-activated carbon composite from coal gangue with enhanced adsorption performance. *Chem. Eng. J.* **2020**, *390*, 124513.
22. Wanyonyi, F.S.; Fidelis, T.T.; Mutua, G.K.; Orata, F.; Pembere, A.M.S. Role of pore chemistry and topology in the heavy metal sorption by zeolites: From molecular simulation to machine learning, *Comput. Mater. Sci.* **2021**, *195*, 110519.
23. Kragović, M.; Pašalić, S.; Marković, M.; Petrović, M.; Nedeljković, B.; Momčilović, M.; Stojmenović, M. Natural and Modified Zeolite—Alginate Composites. Application for Removal of Heavy Metal Cations from Contaminated Water Solutions. *Minerals* **2018**, *8*, 11. [[CrossRef](#)]
24. Abdelrahman, E.A.; Abou El-Reash, Y.G.; Youssef, H.M.; Kotp, Y.H.; Hegazey, R.M. Utilization of rice husk and waste aluminum cans for the synthesis of some nanosized zeolite, zeolite/zeolite, and geopolymer/zeolite products for the efficient removal of Co(II), Cu(II), and Zn(II) ions from aqueous media. *J. Hazard. Mater.* **2020**, *401*, 123813. [[CrossRef](#)]
25. Olegario, E.; Pelicano, C.M.; Felizco, J.C.; Mendoza, H. Thermal stability and heavy metal (As^{5+} , Cu^{2+} , Ni^{2+} , Pb^{2+} and Zn^{2+}) ions uptake of the natural zeolites from the Philippines. *Mater. Res. Express* **2019**, *6*, 085204. [[CrossRef](#)]
26. Wiśniewska, M.; Szewczuk-Karpisz, K.; Ostolska, I.; Terpiłowski, K.; Sternik, D.; Zarko, V.; Gun'ko, V. Comparison of the Poly(vinyl alcohol) Adsorption Behaviour on the Mixed Oxides with Different Surface Structure. *Mater. Sci.* **2016**, *22*, 268–272. [[CrossRef](#)]
27. Wiśniewska, M.; Chibowski, S.; Urban, T.; Fijałkowska, G.; Medykowska, M.; Bogatyrov, V.; Nosal-Wiercińska, A.; Klepka, T.; Szewczuk-Karpisz, K. Modification of Surface Properties of Colloidal Suspensions of $\text{Ni}_x\text{O}_y\text{-SiO}_2$ Mixed Oxides with Different Ni Contents by the Adsorption Layers of Poly(Vinyl Alcohol). *J. Clust. Sci.* **2020**. [[CrossRef](#)]
28. Wiśniewska, M.; Fijałkowska, G.; Ostolska, I.; Franus, W.; Nosal-Wiercińska, A.; Tomaszewska, B.; Goscińska, J.; Wójcik, G. Investigations of the possibility of lithium acquisition from geothermal water using natural and synthetic zeolites applying poly(acrylic acid). *J. Clean. Prod.* **2018**, *195*, 821–830. [[CrossRef](#)]
29. Panek, R.; Wdowin, M.; Bandura, L.; Wisła-Walsh, E.; Gara, P.; Franus, W. Changes in the textural parameters of fly ash-derived Na-P1 zeolite during compaction processes. *Mineralogia* **2017**, *48*, 3–22. [[CrossRef](#)]
30. Wdowin, M.; Franus, M.; Panek, R.; Bandura, L.; Franus, W. The conversion technology of fly ash into zeolites. *Clean Tech. Environ. Policy* **2014**, *16*, 1217–1223. [[CrossRef](#)]
31. Franus, W.; Wdowin, M.; Franus, M. Synthesis and characterization of zeolites prepared from industrial fly ash. *Environ. Monit. Assess.* **2014**, *186*, 5721–5729. [[CrossRef](#)]
32. Bandura, L.; Panek, R.; Madej, J.; Franus, W. Synthesis of zeolite-carbon composites using high-carbon fly ash and their adsorption abilities towards petroleum substances. *Fuel* **2021**, *283*, 119173. [[CrossRef](#)]
33. Sing, K.S.W.; Everett, D.H.; Haul, R.A.W.; Moscou, L.; Pierotti, R.A.; Rouquerol, J.; Siemieniewska, T. Reporting Physisorption Data For Gas/Solid Systems with Special Reference to the Determination of Surface Area and Porosity. *Pure Appl. Chem.* **1985**, *57*, 603–619. [[CrossRef](#)]
34. Thommes, M.; Kaneko, K.; Neimark, A.V.; Olivier, J.P.; Rodriguez-Reinoso, F.; Jean Rouquerol, J.; Sing, K.S.W. Physisorption of gases, with special reference to the evaluation of surface area and pore size distribution (IUPAC Technical Report). *Pure Appl. Chem.* **2015**, *87*, 9–10. [[CrossRef](#)]
35. Ościk, J. *Adsorption*; UMCS: Lublin, Poland, 1969; pp. 91–124. (In Polish)
36. Foo, K.Y.; Hameed, B.H. Insights into the modeling of adsorption isotherm systems. *Chem. Eng. J.* **2010**, *156*, 2–10. [[CrossRef](#)]
37. Ho, Y.S.; McKay, G. Sorption of dye from aqueous solution by peat. *Chem. Eng. J.* **1998**, *70*, 115–124. [[CrossRef](#)]
38. Ho, Y.S.; McKay, G. Application of kinetics models to the sorption of copper(II) onto peat. *Ads. Sci. Technol.* **2002**, *20*, 797–815. [[CrossRef](#)]
39. Homaeigohar, S.; Zillohu, A.U.; Abdelaziz, R.; Hedayati, M.K.; Elbahri, M. A novel nanohybrid nanofibrous adsorbent for water purification from dye pollutants. *Materials* **2016**, *9*, 848. [[CrossRef](#)] [[PubMed](#)]
40. Homaeigohar, S.; Botcha, N.K.; Zarie, E.S.; Elbahri, M. Ups and downs of water photodecolorization by nanocomposite polymer nanofibers. *Nanomaterials* **2019**, *9*, 250. [[CrossRef](#)] [[PubMed](#)]
41. Ho, Y. The kinetics of sorption of divalent metal ions onto sphagnum moss peat. *Water Res.* **2000**, *34*, 735–742. [[CrossRef](#)]
42. Janusz, W. Electrical double layer at the metal oxide–electrolyte interface. In *Interfacial Forces and Fields: Theory and Applications*; Dekker, M., Ed.; CRC Press: New York, NY, USA, 1999; Volume 85, Chapter 4.
43. Oshima, H. A simple expansion for Henry's function for the retardation effect in electrophoresis of spherical colloidal particles. *J. Colloid Interface Sci.* **1994**, *168*, 269–271. [[CrossRef](#)]
44. Lee, M.-G.; Yi, G.; Ahn, B.-J.; Roddick, F. Conversion of coal fly ash into zeolite and heavy metal removal characteristics of the products. *Korean J. Chem. Eng.* **2000**, *17*, 325–331. [[CrossRef](#)]

45. Sahoo, T.R.; Prelot, B. Adsorption processes for the removal of contaminants from wastewater. *Nanomater. Detect. Remov. Wastewater Pollut.* **2020**, *161–222*. [[CrossRef](#)]
46. Sahu, O.; Singh, N. Significance of bioadsorption process on textile industry wastewater. *Impact Prospect. Green Chem. Text. Technol.* **2019**, *367–416*. [[CrossRef](#)]
47. Mu, T.-H.; Sun, H.-N. Sweet Potato Leaf Polyphenols: Preparation, Individual Phenolic Compound Composition and Antioxidant Activity. *Polyphen. Plants* **2019**, *365–380*. [[CrossRef](#)]
48. Trochanowska, J.; Kowalczyk, P.B. *Point of Zero Charge on the Surface of Cuprous Shale in An Aqueous Solution*; Łupek Miedzionośny WGGG PWr: Wrocław, Poland, 2014; pp. 61–64. (In Polish)
49. Wiśniewska, M.; Fijałkowska, G.; Szewczuk-Karpisz, K.; Teresa, U.; Nosal-Wiercińska, A.; Wójcik, G. Comparison of adsorption affinity of anionic and cationic polyacrylamides for montmorillonite surface in the presence of chromium(VI) ions. *Adsorption* **2019**, *25*, 41–50. [[CrossRef](#)]
50. Belova, T.P. Adsorption of heavy metal ions (Cu^{2+} , Ni^{2+} , Co^{2+} and Fe^{2+}) from aqueous solutions by natural zeolite. *Heliyon* **2019**, *5*, e02320. [[CrossRef](#)]
51. Kats, A.M.; Nikashina, V.A.; Bychkova, Y.V. Sorption of heavy metals Ni, Cd, Cr, Zn, Cu from surface water on natural and modified clinoptilolite. *J. Sorpt. Chromatogr. Proc.* **2013**, *13*, 808–815.
52. Visa, M.; Popa, N. Adsorption of heavy metals cations onto zeolite materials from aqueous solution. *J. Membr. Sci. Technol.* **2015**, *5*, 133.
53. Taamneh, Y.; Sharadqah, S. The removal of heavy metals from aqueous solution using natural Jordanian zeolite. *Appl. Water Sci.* **2017**, *7*, 2021–2028. [[CrossRef](#)]
54. Sadek, R.; Chałupka, K.; Dźwigaj, S. Application and synthesis of zeolite materials. *Eliksir* **2015**, *2*, 36–39. (In Polish)
55. Gulicovski, J.J.; Čerović, L.S.; Milonjić, S.K. Point of Zero Charge and Isoelectric Point of Alumina. *Mater. Manuf. Process.* **2008**, *23*, 615–619. [[CrossRef](#)]
56. Bajpai, P. Colloid and Surface Chemistry. In *Biermann's Handbook of Pulp and Paper*; Elsevier: Amsterdam, The Netherlands, 2018; pp. 381–400.
57. Lament, K. *Study on the Mechanism of Adsorption of Ca^{2+} and Fe^{2+} Cations on Metal Oxides Using An Ion-Selective Electrode and A Combined Platinum Electrode*; Maria Curie-Skłodowska University: Lublin, Poland, 2021; pp. 97–102. (In Polish)